

Fractional repetitive control of nanopositioning stages for tracking high-frequency periodic inputs with nonsynchronized sampling

Cite as: Rev. Sci. Instrum. **90**, 055108 (2019); <https://doi.org/10.1063/1.5088673>
Submitted: 13 January 2019 . Accepted: 26 April 2019 . Published Online: 20 May 2019

Linlin Li, Guoying Gu, and LiMin Zhu



View Online



Export Citation



CrossMark

ARTICLES YOU MAY BE INTERESTED IN

[Model reference adaptive damping control for a nanopositioning stage with load uncertainties](#)

Review of Scientific Instruments **90**, 045101 (2019); <https://doi.org/10.1063/1.5064722>

[Invited Review Article: High-speed flexure-guided nanopositioning: Mechanical design and control issues](#)

Review of Scientific Instruments **83**, 121101 (2012); <https://doi.org/10.1063/1.4765048>

[A fast and accurate piezoelectric actuator modeling method based on truncated least squares support vector regression](#)

Review of Scientific Instruments **90**, 055004 (2019); <https://doi.org/10.1063/1.5086491>



Your Qubits. Measured.

Meet the next generation of quantum analyzers

- Readout for up to 64 qubits
- Operation at up to 8.5 GHz, mixer-calibration-free
- Signal optimization with minimal latency

[Find out more](#)



Fractional repetitive control of nanopositioning stages for tracking high-frequency periodic inputs with nonsynchronized sampling

Cite as: Rev. Sci. Instrum. 90, 055108 (2019); doi: 10.1063/1.5088673
Submitted: 13 January 2019 • Accepted: 26 April 2019 •
Published Online: 20 May 2019



Linlin Li,¹ Guoying Gu,¹ and LiMin Zhu^{1,2,a)}

AFFILIATIONS

¹State Key Laboratory of Mechanical System and Vibration, School of Mechanical Engineering, Shanghai Jiao Tong University, Shanghai 200240, China

²Shanghai Key Lab of Advanced Manufacturing Environment, Shanghai, China

^{a)}Electronic mail: zhulm@sjtu.edu.cn

ABSTRACT

The repetitive control (RC) has been employed for high-speed tracking control of nanopositioning stages due to its abilities of precisely tracking periodic trajectories and rejecting periodic disturbances. However, in digital implementation, the sampling frequency should be integer multiple of the tracking frequency of the desired periodic trajectory. Otherwise, the rounding error would result in a significant degradation of the tracking performance, especially for the case of high input frequencies. To mitigate this rounding effect, the fractional repetitive control (FRC) technique is introduced to control the nanopositioning stage so as to precisely track high-frequency periodic inputs without imposing constraints on the sampling frequency of the digital control system. The complete procedure of controller design and implementation is presented. The techniques to deal with the problems of non-minimum phase system and fractional delay points number are described in detail. The proposed FRC is plugged into the proportional-integral control, and implemented on a custom-built piezo-actuated nanopositioning stage. Validation experiments are conducted, and the results show that the tracking errors caused by the rounding effect in the traditional RC approach are almost completely eliminated, when tracking sinusoidal waveforms with frequencies from 1000 Hz to 1587.3 Hz under the sampling frequency of 50 kHz, where the fractional parts being rounded vary from 0 to 0.5.

Published under license by AIP Publishing. <https://doi.org/10.1063/1.5088673>

I. INTRODUCTION

Piezo-actuated nanopositioning stages are the important components of the nanomanufacturing equipment and nanomeasurement instruments, such as nanolithography facilities¹ and scanning probe microscopes.² A typical piezo-actuated nanopositioning stage is composed of the piezoelectric actuator, compliant mechanism, displacement sensor, and control system.³ To achieve high-speed and high precision operations, the stage mainly faces two challenges. The first challenge is the inherent hysteresis nonlinearity of the piezoelectric actuator.^{4–6} It is amplitude-dependent and rate-dependent, which can cause the positioning errors up to 15% of the moving range in the open-loop control.⁷ The second challenge is the lightly damped resonant modes of the compliant mechanism.^{4,5} They can be easily excited during high-speed tracking and thus can cause vibrations and large positioning errors. These two problems are usually addressed independently.^{8–11} In fact, they are commonly

coupled together, especially in high-speed operations, which makes the control design complex and challenging.^{12,13}

In many real-time applications, the nanopositioning stages are configured to fulfill the periodic operations. Take atomic force microscope as an example, the general raster/sinusoidal scanning motions are realized with the periodic triangular/sinusoidal trajectory of one lateral axis and the corresponding staircase trajectory of the other one lateral axis,^{4,14–18} in which the primary objective is to minimize the tracking errors of the periodic trajectories.^{12,13} Nowadays, with its remarkable performances of tracking periodic trajectories and rejecting periodic disturbances, the repetitive control (RC) has attracted researchers' attention in such applications. In digital implementation, as an internal model control method, the RC can be expressed as $1/(z^N - 1)$ (N is the number of delay points in one period of the reference trajectory), which generates infinite gains at the fundamental frequency and its harmonics.¹⁹ In order to improve the robustness of the RC, the phase

compensator and low-pass filter are incorporated into the RC to obtain a better tracking performance.^{20–22} It is found that when the nanopositioning stage operates in periodic applications, the hysteresis and vibration induced tracking errors are also periodic.^{12,23} Therefore, the RC provides a solution to compensate for both the hysteresis and the dynamics effects of the piezo-actuated nanopositioning stages. In our most recent work, it is shown that the hysteresis nonlinearity mainly affects the system at the odd-harmonics of the input signals and an odd-harmonic RC is then developed.¹² Despite the faster convergence and lower computation cost of the odd-harmonic RC, the even-harmonic tracking errors still exist and are even amplified, which leads to the relatively larger tracking errors as compared with the conventional RC.²⁴ Besides, it is worthy of mentioning that the convergence time of the RC is slightly longer than that of the odd-harmonic RC, not the two times in theory during high-speed operations. In this sense, the RC is the promising technique for precision tracking control of nanopositioning stages with high input frequencies.

In practical applications, there exists a physical limitation for the implementation of the RC technique. It is obvious that the number of delay points in the RC technique should be a positive integer, which implies that the sampling frequency must be integer multiple of the tracking frequency of the desired trajectory. However, this rigorous condition cannot be always satisfied in some specific applications. One typical case is the Lissajous trajectory tracking application,^{25,26} where the ratio of the delay points numbers of the two lateral axes is $(2M - 1)/2M$ ($M > 1$ is an integer) to guarantee the Lissajous trajectory returns to its starting point. In such case, it would cause a fractional delay points number for one of the two lateral axes, especially with high input frequencies, which hinders the application of the RC technique. Although one can choose a sampling frequency that is a multiple of the least common multiple of the individual scanning axis frequencies to ensure that the numbers of the delay points for the two axes are both integer, it requires a much higher sampling frequency. Additionally, this strategy requires the remodeling of the system and redesign of the controller, which is quite inconvenient. Another simple solution to this problem is rounding the number of fractional delay points to the nearest integer,²⁷ i.e., $N = \text{round}(\hat{N})$ is employed to implement the RC. Although this rounding errors can be ignored for low frequency inputs, it would lead to significant tracking errors in high-speed tracking tasks. It will be shown in this work that for high-speed tracking applications, the rounding effect would result in the tracking errors up to 5%, which degrades the tracking performance severely.

In this article, the idea of fractional repetitive control (FRC) is introduced to control the nanopositioning stage so as to precisely track high frequency periodic inputs without imposing constraints on the sampling frequency of the digital control system. Although the FRC technique was recently developed in the field of power-conditioning systems,^{27–30} to our best knowledge, this is the first attempt at applying the FRC to control the nanopositioning stage, which is a non-minimum phase system with complicated hysteresis nonlinearity.

The remainder of this article is arranged as follows. In Sec. II, the FRC design and implementation are presented. In Sec. III, the experimental setup and controller parameters design are presented. The effectiveness of the FRC technique on high-speed tracking control is demonstrated by comparative experiments in Sec. IV. The conclusion is summarized in the last section.

II. CONTROLLER DESIGN

A. Fractional repetitive control design

As investigated in the previous works,^{12,23} the nanopositioning stage can be described as a time-invariant linear plant with a bounded input disturbance resulting from the hysteresis nonlinearity, and for a periodic reference input, this disturbance is also periodic. Hence, the RC can be designed based on the linear dynamics to account for the tracking errors caused by both the hysteresis disturbance and the vibrational dynamics. It avoids the construction of the complicated hysteresis model and its inversion. It should be noted that since the model of the nanopositioning stage is a non-minimum phase system with complicated hysteresis nonlinearity, the RC technique developed in our previous work¹² is employed as the prototype of the FRC, which is different from those employed in other applications.^{28,29} The block diagram of the FRC is shown in Fig. 1, in which the fractional repetitive controller $C_{FRC}(z)$ is plugged into the baseline feedback controller $C_f(z)$. The items $y_d(k)$, $y_a(k)$, and $e(k)$ are the desired reference trajectory, the actual output displacement, and the corresponding tracking error, respectively. The fractional repetitive controller $C_{FRC}(z)$ is composed of the repetitive loop $z^{-\hat{N}}$, the control gain k_c , the phase compensator z^m , and the closed-loop system inversion $C_i(z)$. $\hat{N} = f_s/f_n$ is termed as the delay points number, where f_n and f_s denote the tracking frequency and the sampling frequency, respectively. To improve the control robustness, there is a low pass filter $Q(z) = (az + b + az^{-1})^i$ incorporated in the repetitive part, where the parameters satisfy the condition $2a + b = 1$, and i is an integer to adjust the bandwidth of the low-pass filter. The

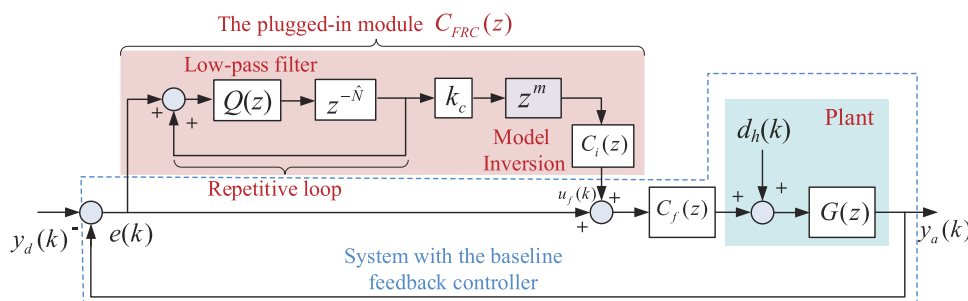


FIG. 1. The block diagram of the control system with the plugged-in fractional repetitive control.

closed-loop system inversion $C_i(z)$ satisfies

$$C_i^{-1}(z) = \frac{G(z)C_f(z)}{1 + G(z)C_f(z)}. \quad (1)$$

Due to the non-minimum phase nature of the nanopositioning stage, the inversion $C_i(z)$ cannot be derived directly. Therefore, the zero-phase-tracking-error method³¹ is employed to calculate the closed-loop system inversion. For convenience, Eq. (1) is rewritten as

$$C_i^{-1}(z) = z^{-d} \frac{B_u(z)B_s(z)}{A(z)}, \quad (2)$$

where $B_u(z)$ contains all the zeros that locate out of the unit circle in z -plane, $B_s(z)$ contains the other zeros, $A(z)$ is the denominator of the close-loop system transfer function, and d denotes the relative degree of $C_i^{-1}(z)$. The approximate closed-loop system inversion has the following expression:

$$C_i(z) = z^{-(n_c+n_u)} \frac{B_f(z)A(z)}{B_s(z)\beta}, \quad (3)$$

where

$$\beta \geq \max_{\omega \in [0, \pi]} (|B_u(e^{-j\omega})|^2). \quad (4)$$

In this work, the parameter β is set as $\beta = |\beta_0| + |\beta_1| + |\beta_2| + \dots$, where β_i , $i = 1, 2, \dots$ are the corresponding coefficients of $B_u(z)$.¹⁹ $B_f(z)$ is obtained by flipping the coefficients of $B_u(z)$, and n_u represents the order of the unstable transfer function $B_u(z)$, and n_c is an integer introduced to keep the controller causal for physical implementation. The order of the phase compensator z^m in Fig. 1 is set as $m = d + n_c$.

Because the item z^m is physically unrealizable, this item is integrated into the repetitive loop for real-time implementation. The equivalent control diagram of the FRC is shown in Fig. 2.

B. Fractional repetitive control implementation

Since this work focuses on the rounding effect caused by the nonsynchronized sampling, the fractional delay points number \hat{N} is considered. The corresponding fractional delay $z^{-\hat{N}}$ is physically unrealizable in real applications. To address this problem, the Lagrange interpolating approach is employed to approximate the fractional part of $z^{-\hat{N}}$.²⁷⁻²⁹ Let $N^* = \text{round}(\hat{N} - n/2)$ and $\alpha = \hat{N} - N^*$ denote the major integer part and the residual fractional part of the delay points number, respectively, where n is the order of the Lagrange interpolating. Then, the fractional delay part $z^{-\alpha}$ can be approximately expressed as

$$z^{-\alpha} \approx \sum_{k=0}^n A_k z^{-k}, \quad (5)$$

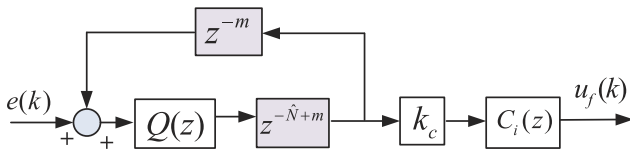


FIG. 2. The equivalent block diagram of the fractional repetitive control for physical implementation.

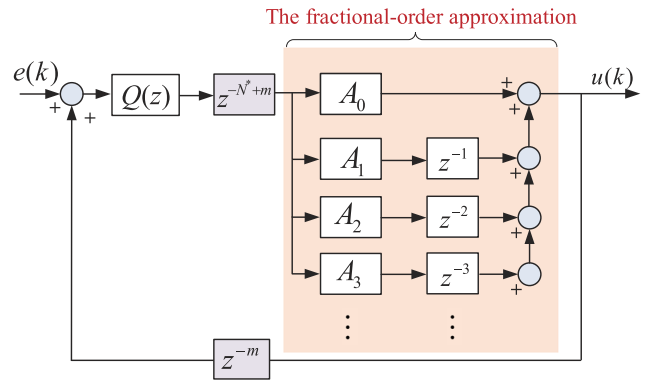


FIG. 3. The implementation of the delay loop in the FRC with the Lagrange interpolating approach.

where

$$A_k = \prod_{i=0, i \neq k}^n \frac{\alpha - i}{k - i}, \quad k = 0, 1, 2, \dots, n \quad (6)$$

are the Lagrange coefficients. Thus, the complete fractional delay part has the expression

$$z^{-\hat{N}} \approx z^{-N^*} \times z^{-\alpha} \approx z^{-N^*} \times \sum_{k=0}^n A_k z^{-k}. \quad (7)$$

The block diagram of the realizable fractional delay loop within the FRC is illustrated in Fig. 3, where the fractional part is approximated by sum of the integer delay branches for practical implementation.

Basically, the higher the Lagrange interpolation order is, the more accurate the approximated fractional delay part will be. Normally, the Lagrange interpolation order is not greater than 5, because a higher order would result in the unwanted oscillations of the interpolants.³² From the viewpoint of digital signal processing, the Lagrange interpolating may be regarded as the

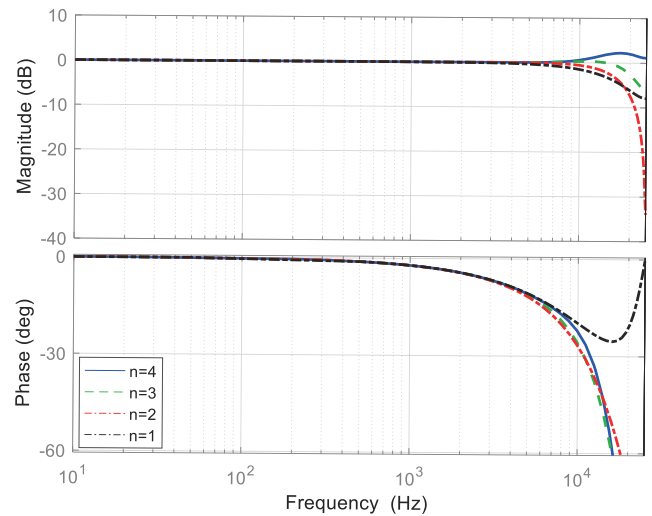


FIG. 4. The magnitude and phase responses of the fractional delay with different interpolation orders.

finite impulse response (FIR) low-pass filtering. The magnitude and phase response of the equivalent FIR filters for $n = 1, 2, 3$, and 4 are compared for a specific fractional delay $\alpha = 0.3$ in Fig. 4. As can be seen, the magnitude and phase responses for different orders are nearly same in the frequency band below 3000 Hz. Comparatively, the responses with $n = 3$ and $n = 4$ exhibit better high-frequency performance. In this work, n is selected as 3 since it is adopted in most applications.^{28,29}

III. EXPERIMENTAL SYSTEM DESCRIPTION

A. Experimental setup

To verify the effectiveness of the developed FRC technique, one custom-built piezo-actuated flexible-kinematic two-dimensional nanopositioning stage is employed as the testing platform in this work. As shown in Fig. 5, this experimental setup mainly consists of four components, which are the stage, the dSPACE control module, the voltage amplifier, and the gauging module. The workspace of the stage is $11.2 \mu\text{m} \times 11.6 \mu\text{m}$, the first-order resonant frequency is over 13.6 kHz, and the maximum cross-coupling between the X- and Y-axes is lower than 0.52%. Because the stage has nearly decoupled performance, the Y-axis of the stage is employed as the testing axis. The dSPACE-DS1103 control module is equipped to generate the reference signals and capture the displacement signals of the stage for close-loop control. This control module is configured with digital to analog converters (DACs) and analog to digital converters (ADCs) for transferring the signals. The DACs could generate the analog control voltage to the voltage amplifier for generating the actuation voltage in the range of 0–200 V. The measurement module could capture the displacements signals from the capacitive sensor and transfer it to the ADCs in the range of -1 V to 1 V . Two capacitive sensors (Probe 2823 and Gauging Module 8810 designed by MicroSense, US, range of $\pm 25 \mu\text{m}$, resolution $< 1 \text{ nm} - \text{rms}$) are employed to measure the real-time displacements signals of the end-effector of the stage. The sampling frequency of the dSPACE control is set as 50 kHz. For more

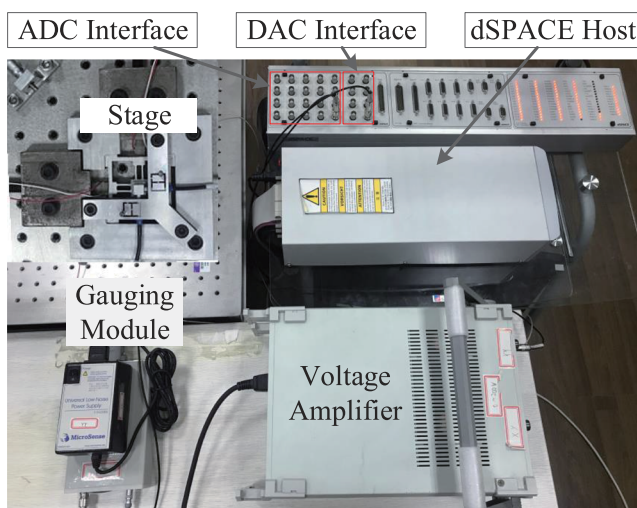


FIG. 5. The experimental setup.

information of the experimental setup, readers could refer to our previous work.³³

B. System identification

With the objective of identifying the system dynamics and eliminating the hysteresis influence, the band-limited white noise signals with low amplitude are utilized to excite the stage. The actuation noise signals and the actual displacement signals are captured simultaneously, which are utilized to identify the dynamics of the stage with the help of the MATLAB system identification ToolBox. The ARX algorithm and the least square method are employed in the identification process. It is worthy of mentioning that the higher the order of the identified dynamics is, the more accurate the identified model is. However, high order model would result in great complexity in controller design and implementation, especially in inversion calculation in the proposed control scheme. Hence, with the trade-off of the identification accuracy and computational complexity, the system dynamics is determined as

$$G(z) = \frac{-5.662e^{-5}z^5 + 0.0005z^4 + 0.0038z^3 + 0.0509z^2 + 0.1149z + 0.1032}{z^6 - 0.4354z^5 + 1.013z^4 - 0.6771z^3 + 0.3096z^2 + 0.1197z} \quad (8)$$

With the spectrum analysis, the experimental results and the identified model are compared in Fig. 6. It can be seen that the identified system dynamics could describe the stage precisely in a wide range of frequencies, which bases the following controller design.

C. Controller parameters design and performance evaluation

Owing to its easy implementation, the baseline feedback controller $C_f(z)$ is chosen as the widely employed discrete-time proportional-integral (PI) controller. The PI controller has the transfer function of $C_f(z) = k_p + \frac{k_i T_s}{z-1}$, where k_p and k_i are the proportional and integral gains, respectively. The two control gains are

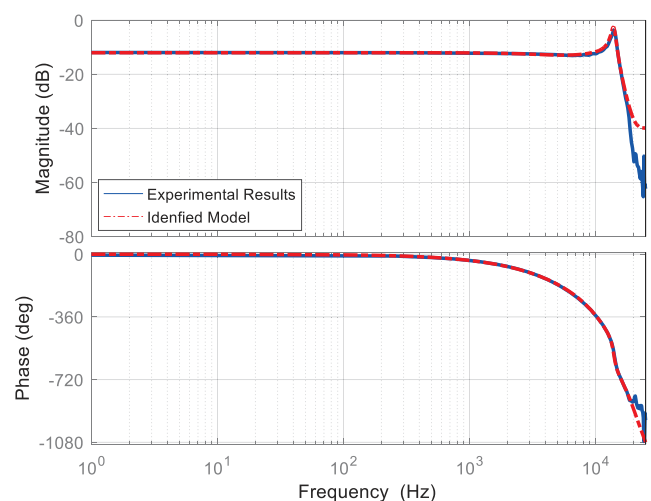


FIG. 6. The comparison of the experimental results with the identified model.

determined as $k_p = 0.1$, $ki = 6000$, with the trial and error method by experiments. Based on the identified dynamics $G(z)$, the closed-loop system inversion $C_i(z)$ can be determined according to Eq. (3), where d , n_c , and n_u are calculated as 1, 5, and 5, respectively. Therefore, the order of phase compensator z^m is deduced as 6. The parameters of the low-pass filter $Q(z)$ are set as $a = 0.25$, $b = 0.5$, and $i = 1$. The control gain k_c is optimized as 1 following the simulation results.

To evaluate the performance of the FRC, the sensitivity functions under different control schemes are investigated for tracking a specific periodic trajectory. It is worthy of noting that when \hat{N} is an integer, the FRC is reduced to the RC. To demonstrate the advantages of the FRC over the RC, the basic control parameters of the RC are chosen the same as those of the FRC in Fig. 1, except for the number of delay points. Since the main focus of this work is the high-speed tracking control in the case of nonsynchronized sampling, the tracking frequency of 1100 Hz is studied in detail, which provides the fractional delay points number $\hat{N} \approx 45.45$. In this case, the two delay points number of the FRC are $N^* = 44$, $\alpha = 1.45$, while the delay points number of RC is 45 for implementation. The sensitivity functions of PI + FRC, PI + RC, and PI control are compared in Fig. 7. It is shown clearly that both the PI + RC scheme and the PI + FRC scheme can improve the tracking performance of the stage, as compared with the PI scheme. The rounding effect of the RC technique results in the reduction of rejection capability from -45 dB to -22 dB at the frequency of 1100 Hz, as compared with the FRC technique. This degradation of rejection capability also occurs at the harmonic frequencies. Although it can still reduce the tracking errors to some extent, the RC technique could not mitigate the tracking errors at the tracking frequency of 1100 Hz completely. Meanwhile, it can be observed that the larger deviation between the target tracking frequency and the rounded tracking frequency, the larger the tracking errors will be. By contrast, the approximated PI + FRC scheme exhibits an excellent tracking errors rejection ability at the target tracking frequencies.

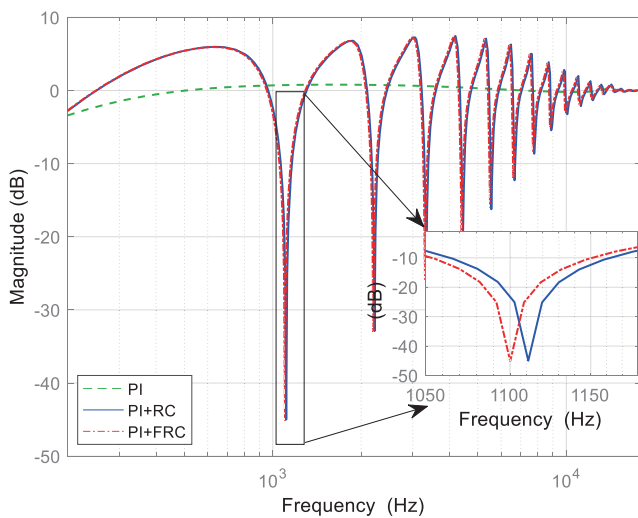


FIG. 7. The comparison of sensitivity functions of different control schemes for the tracking frequency of 1100 Hz.

IV. EXPERIMENTAL RESULTS

To demonstrate the effectiveness of the proposed PI + FRC scheme on mitigating the rounding effect, experiments of tracking sinusoidal trajectories with the amplitude of $1.25 \mu\text{m}$ and different frequencies are carried out on the experimental nanopositioning stage. The PI and PI + RC control schemes are chosen for comparisons. To quantitatively evaluate the tracking performance, the maximum tracking errors e_{max} and the root-mean-square tracking errors e_{rms} defined as

$$e_{max} = \max_{t \in (0, 10T]} |y_d(t) - y_a(t)|, \quad (9)$$

$$e_{rms} = \sqrt{\frac{1}{10T} \sum_{t \in (0, 10T]} [y_d(t) - y_a(t)]^2}. \quad (10)$$

All the experimental results are summarized in Table I. It is observed that the tracking errors of the PI + RC scheme with the 100 Hz input frequency, which do not suffer from the rounding effect, are a little smaller than those of the PI + RC scheme with the 150 Hz input frequency, but similar to those of the PI + FRC scheme with same input frequency. These results indicate that the tracking errors caused by the rounding effect of the RC are very low for the low input frequency. However, it is found that the tracking errors of the PI + RC scheme with the 1000 Hz and 1562.5 Hz input frequencies, both of which do not suffer from the rounding effect, are much smaller than those of the PI + RC scheme with the 1100 Hz, 1200 Hz, 1300 Hz, 1400 Hz, and 1500 Hz input frequencies, but similar to those of the PI + FRC scheme with the same input frequencies. When the input frequency goes from 1000 Hz to 1500 Hz, the tracking errors of the PI + FRC scheme grow incrementally. However, the tracking errors of the PI + RC scheme do not exhibit a regular tendency due to the irregularity of the rounding errors in the chosen frequencies. These results indicate that the tracking errors caused by the rounding effect of the RC are significant for the high input frequency, and these errors can be almost eliminated by the FRC.

In particular, the experiments of tracking sinusoidal signals with the frequencies near 1562.5 Hz ($N = 32$) are further conducted and investigated in detail. Two specific cases of 1587.3 Hz ($\hat{N} = 31.5$) and 1538.5 Hz ($\hat{N} = 32.5$) are taken into account. The number of delay points N for RC technique are set as 32 for both two cases. The integer delay points numbers for the FRC scheme \hat{N} are set as 30 and 31, respectively, while the fractional parts of FRC scheme are both determined as 1.5. The tracking results of the PI control, PI + RC, and PI + FRC schemes for the two frequencies are shown in Figs. 8(A) and 8(B), respectively. From the tracking errors results in Figs. 8(A-b) and 8(B-b), it is obvious that, compared with the PI control, both the RC and FRC schemes improve the tracking performance significantly. Due to the rounding effect, the maximum tracking errors of the PI + RC scheme in Fig. 8(A-c) in steady state are about $0.1298 \mu\text{m}$, which are much larger than the results of $0.0149 \mu\text{m}$ corresponding to the input frequency of 1562.5 Hz as shown in Table I that does not suffer from the rounding effect. With the consideration of the fractional delay part, the tracking errors of the RC are reduced about 88% and the rounding effect is almost mitigated, which validated the approximation accuracy of the Lagrange interpolating method used in the FRC. Also, it can be observed that

TABLE I. The tracking errors under different control schemes for different tracking frequencies (where N and \hat{N} are the numbers of delay points in the repetitive loop).

Frequency (Hz)	PI		PI + RC		N	PI + FRC		
	e_{max} (μm)	e_{rms} (μm)	e_{max} (μm)	e_{rms} (μm)		e_{max} (μm)	e_{rms} (μm)	\hat{N}
100	0.4210	0.2854	0.0052	0.0013	500
150	0.6225	0.4230	0.0062	0.0025	333	0.0050	0.0013	333.33
1000	1.4330	1.0130	0.0097	0.0038	50
1100	1.4313	1.0084	0.0798	0.0514	45	0.0103	0.0044	45.45
1200	1.4292	1.0090	0.0667	0.0425	42	0.0103	0.0051	41.66
1300	1.4259	1.0090	0.0926	0.0622	38	0.0111	0.0059	38.46
1400	1.4215	1.0054	0.0670	0.0430	36	0.0119	0.0067	35.71
1500	1.4169	0.9988	0.0798	0.0523	33	0.0143	0.0077	33.33
1562.5	1.4101	1.0012	0.0149	0.0078	32

the convergence speed of the PI + FRC scheme is as fast as that of the PI + RC scheme from Fig. 8.

The other control objective of the RC technique is to mitigate the complicated hysteresis nonlinearity under periodic operations, which is usually coupled with the linear dynamics of the mechanism. Commonly, such nonlinearity becomes more severe with the increase of input frequency. Again, the tracking frequencies near 1562.5 Hz are considered, where the severe hysteresis nonlinearity in the open-loop control is shown clearly in Fig. 9, for the input frequencies of 1587.3 Hz and 1538.5 Hz. To better verify the

effectiveness of the FRC to compensate for both the hysteresis and the dynamics effects of the piezo-actuated nanopositioning stages in the case of nonsynchronized sampling, the relations between the actual and desired displacements under different control schemes for tracking sinusoidal waveforms with frequencies of 1587.3 Hz and 1538.5 Hz are plotted in Figs. 9(a) and 9(b), respectively. It can be seen that, with only PI control, the nonlinearity effect is still very serious. On the other hand, although the periodic tracking errors caused by the hysteresis and linear dynamic effects are mitigated greatly with the RC technique, they cannot be compensated

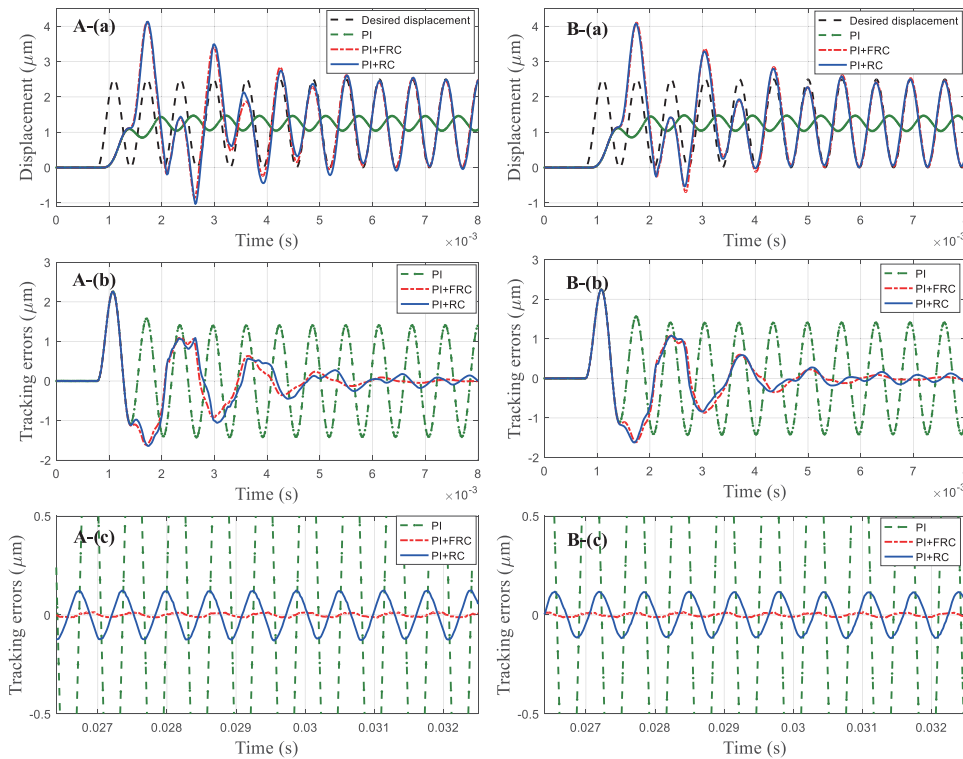


FIG. 8. The sinusoidal trajectory tracking results for different control schemes: (A) the tracking frequency of 1587.3 Hz; (B) the tracking frequency of 1538.5 Hz; (a) the overall of the tracking results; (b) the tracking errors; (c) the tracking errors in the steady state.

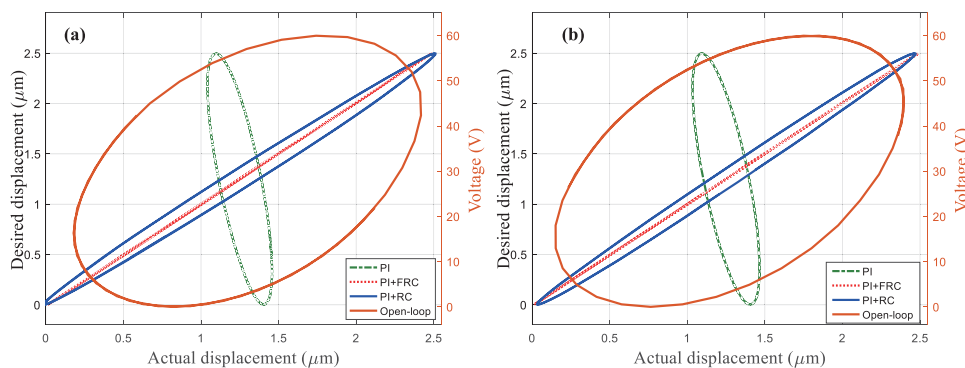


FIG. 9. The relations between the actual and desired displacements under different control schemes: (a) 1587.3 Hz; (b) 1538.5 Hz.

completely due to the inherent rounding effect. By contrast, with the FRC technique, the residual nonlinear effect is well eliminated, and the input-output relation of the system is almost linear. These results demonstrate that the FRC can well compensate for the hysteresis and dynamics effects of the nanopositioning stage without imposing constraints on the sampling frequency of the digital control system.

V. CONCLUSION

This article introduced for the first time the FRC strategy to handle the rounding effect met in high-speed tracking control of nanopositioning stage using the RC technique. The techniques to deal with the problems of non-minimum phase system and fractional delay points are described in detail. The proposed FRC is plugged into a PI control and implemented on a custom-built piezo-actuated nanopositioning stage. The experimental results show that the tracking errors caused by the rounding effect in the traditional RC approach can be mitigated significantly when tracking sinusoidal waveforms with frequencies from 1000 Hz to 1587.3 Hz. With this FRC, the task-dependent constrain on the sampling frequency of the digital control system is no longer required, making the control of the nanopositioning stage more flexible and convenient.

REFERENCES

- F. Dinelli, C. Menozzi, P. Baschieri, P. Facci, and P. Pingue, *Nanotechnology* **21**, 075305 (2010).
- Y. F. Dufre, T. Ando, R. Garcia, D. Alsteens, D. Martinez-Martin, A. Engel, C. Gerber, and D. J. Mller, *Nat. Nanotechnol.* **12**, 295 (2017).
- Y. K. Yong, S. O. R. Moheimani, B. J. Kenton, and K. K. Leang, *Rev. Sci. Instrum.* **83**, 121101 (2012).
- M. S. Rana, H. R. Pota, and I. R. Petersen, *IEEE Trans. Autom. Sci. Eng.* **14**, 1265 (2017).
- G.-Y. Gu, L.-M. Zhu, C.-Y. Su, H. Ding, and S. Fatikow, *IEEE Trans. Autom. Sci. Eng.* **13**, 313 (2016).
- S. Xie and J. Ren, *Rev. Sci. Instrum.* **89**, 076103 (2018).
- G.-Y. Gu, M.-J. Yang, and L.-M. Zhu, *Rev. Sci. Instrum.* **83**, 065106 (2012).
- Z. Li, J. Shan, and U. Gabbert, *IEEE/ASME Trans. Mech.* **23**, 966 (2018).
- A. J. Fleming, *IEEE/ASME Trans. Mech.* **15**, 433 (2010).
- J. Gan, X. Zhang, and H. Wu, *AIP Adv.* **6**, 065204 (2016).
- J. Gan and X. Zhang, *Rev. Sci. Instrum.* **89**, 115002 (2018).
- C.-X. Li, G.-Y. Gu, L.-M. Zhu, and C.-Y. Su, *Sens. Actuators, A* **244**, 95 (2016).
- Y. Wu and Q. Zou, *IEEE Trans. Control Syst. Technol.* **15**, 936 (2007).
- S. Awtar and G. Parmar, *J. Mech. Rob.* **5**, 021008 (2013).
- A. J. Fleming, B. J. Kenton, and K. K. Leang, *Ultramicroscopy* **110**, 1205 (2010).
- Y. R. Teo, Y. Yong, and A. J. Fleming, *Asian J. Control* **20**, 1352 (2018).
- Y. Shan and K. K. Leang, *IEEE Control Syst. Mag.* **33**(6), 86 (2013).
- G. Schitter, K. J. Astrom, B. E. DeMartini, P. J. Thurner, K. L. Turner, and P. K. Hansma, *IEEE Trans. Control Syst. Technol.* **15**, 906 (2007).
- M. Tomizuka, T.-C. Tsao, and K.-K. Chew, *J. Dyn. Syst., Meas., Control* **111**, 353 (1989).
- B. Han, J. S. Lee, and M. Kim, *IEEE Trans. Ind. Electron.* **65**, 2356 (2018).
- C.-Y. Lin and P.-Y. Chen, *Mechatronics* **21**, 239 (2011).
- B. Zhang, D. Wang, K. Zhou, and Y. Wang, *IEEE Trans. Ind. Electron.* **55**, 1595 (2008).
- U. Aridogan, Y. Shan, and K. K. Leang, *J. Dyn. Syst., Meas., Control* **131**, 061103 (2009).
- K. Zhou, D. Wang, B. Zhang, and Y. Wang, *IEEE Trans. Ind. Electron.* **56**, 784 (2009).
- A. Bazaie, Y. K. Yong, and S. O. R. Moheimani, *Rev. Sci. Instrum.* **83**, 063701 (2012).
- T. Tuma, J. Lygeros, V. Kartik, A. Sebastian, and A. Pantazi, *Nanotechnology* **23**, 185501 (2012).
- C. Xie, X. Zhao, M. Savaghebi, L. Meng, J. M. Guerrero, and J. C. Vasquez, *IEEE J. Emerging Sel. Top. Power Electron.* **5**, 809 (2017).
- M. Cheng, Z. Zou, Z. Wang, and K. Zhou, *IET Power Electron.* **7**, 431 (2014).
- Z. Liu, B. Zhang, and K. Zhou, *IEEE Trans. Ind. Electron.* **64**, 7132 (2017).
- T. Liu, D. Wang, and K. Zhou, *IEEE Trans. Power Electron.* **31**, 2669 (2016).
- M. Tomizuka, *J. Dyn. Syst., Meas., Control* **109**, 65 (1987).
- W. Gautschi, *Numerical Analysis*, 2nd ed. (Springer/Birkhauser, New York, 2012).
- C.-X. Li, G.-Y. Gu, M.-J. Yang, and L.-M. Zhu, *Rev. Sci. Instrum.* **84**, 125111 (2013).